ADVANCED OPTICAL MATERIALS

www.advopticalmat.de

Manipulation of the Photonic Spin Hall Effect with High Efficiency in Gold-Nanorod-Based Metasurfaces

Zhancheng Li, Wenwei Liu, Hua Cheng, Shuqi Chen,* and Jianguo Tian*

The photonic spin Hall effect (PSHE) has attracted great interest of the scientific community because of the wide range of spin-controlled nanophotonics applications that it can provide. However, the PSHE is very weak in the reflection and refraction at an interface because of the extremely small spin–orbit interaction. Here, a significant photonic spin Hall effect is reported exhibiting over 70% efficiency in refraction by a gold-nanorod-based metasurface. Moreover, the spin-dependent wave-vector and beam-centroid shifts of the converted refracted waves can be manipulated effectively by changing the periodic length of the proposed metasurface and the transmission distance, respectively. The results suggest intriguing possibilities for manipulating photon spins and orbital angular momentum for applications in nanophotonics and optical communications.

The phenomenon of spin–orbit interaction (SOI) of light recently has attracted significant attention.[1–5] The SOI of light is analogous to the SOI of relativistic quantum particles and electrons in solids with a spatial scale on the order of the wavelength of light. Thus, traditional geometrical optics always neglects wavelength-scale SOI phenomena. The development of nanophotonics and plasmonics has revealed the important role SOI phenomena play at subwavelength scales and has brought novel functionalities to optical nanodevices. The PSHE, which manifests itself in the interplay between the photon spin (polarization) and orbital angular momentum (trajectory) of light, is one of the basic classes of numerous spin–orbit interactions phenomena. The PSHE has attracted growing interest in modern nanophotonics because of its crucial role in determining the behavior of light at subwavelength scales. Traditional approaches to generate the PSHE always are associated with the evolution of the propagation direction of light, which is induced by the geometric Rytov–Vladimirskii–Berry (RVB) phase.[6–9] However, the instances of the PSHE measured in these approaches generally are very weak, and the induced spin-dependent subwavelength shifts are also exceedingly tiny. The diminutive nature of these phenomena prevents their use in real applications in nanophotonics.

Dr. Z. Li, Dr. W. Liu, Prof. H. Cheng, Prof. S. Chen, Prof. J. Tian
The Key Laboratory of Weak Light Nonlinear Photonics
Ministry of Education
School of Physics and TEDA Institute of Applied Physics
Nankai University
Tianjin 300071, China
E-mail: hcheng@nankai.edu.cn; schen@nankai.edu.cn

DOI: 10.1002/adom.201700413

Recent advances in understanding metasurfaces provide an alternative method for overcoming the drawbacks of traditional approaches and for realizing large manifestations of the PSHE.[10,11] Metasurfaces are periodic single-layer artificial nanostructure arrays with subwavelength unit cells and thicknesses that can produce spin-dependent phase gradients. Such phase gradients result in giant instances of the PSHE with spin-dependent wave-vector shifts.[12–26] Ling et al. proposed a giant photonic SHE in a dielectric-based metamaterial.[15] Luo et al. produced a reflective metasurface that generated a giant PSHE with nearly 100% efficiency.[24] Even though numerous approaches for fabricating metasurfaces to yield giant PSHEs and enhanced SOIs have been proposed, the achievement of effective manipulation of the PSHE with high efficiency in refraction, which is quite useful in practice, is still eagerly anticipated by the scientific community. Researchers expect such advances to yield numerous possibilities for applications, such as optical wave-propagation control, optical manipulation enhancement, and structured optical-field generation without suffering interferences with normal-field background.

Here, we present a new approach to manipulating photon spin and orbital angular momentum by introducing the anisotropic optical resonance mode of a gold nanorod. We achieve a giant PSHE in refraction with efficiency over 70% at 1067 nm by using a gold-nanorod-based metasurface. Theoretical analysis shows that the nanorods treated as near-perfect half-wave plates can be used to produce a PSHE with efficiency approaching 100%. Simulation results verify this theoretical prediction and indicate that a giant PSHE can be realized at a wavelength of 1067 nm. The ohmic losses in proposed metasurfaces are quite small and the efficiency of the PSHE approaches to that in metasurfaces designs based on dielectric materials. The realizing of anisotropic optical resonance with π phase delay and the reducing of ohmic losses in the proposed near-perfect half-wave plate overcome the drawbacks of metasurfaces based on metal, which is attributed to a new underlying physics and is quite meaningful for further designs of metasurfaces. In addition, in proposed metasurface, such incident light with an arbitrary polarization state can undergo nearly complete conversion into two refracted waves with opposite spin states and opposite spin-dependent wave-vector shifts. Moreover, the spin-dependent wave-vector shifts and the beam-centroid shifts of the converted refracted waves can be manipulated effectively by

changing the periodic length of the proposed metasurface and the transmission distance, respectively. Further analysis reveals that a giant PSHE can be produced at an arbitrary wavelength by varying the configurations of the structural parameters of the nanorod. This outcome may have a profoundly positive impact on the method's practical applications.

Let us first give a brief review of the PSHE based on the geometric phase gradient. The above approach states that a metasurface can provide partial conversion of the polarization state of incident waves. It can also generate a 0–2π continuous geometric phase gradient along the direction perpendicular to the wave propagation for cross-polarized waves. This generated phase gradient with circular polarization is achieved by rotating the unit cell of the metasurface array along the geometric axis parallel to the wave-propagation direction from 0 to π.[27,28] The introduction of the geometric phase gradient produces anomalous refraction. Then, the relation between the incident and anomalous refraction angles θ_i and θ_t, respectively, can be obtained from the generalized Snell's law

$$n_t \sin\theta_t - n_i \sin\theta_i = \frac{\lambda_o}{2\pi}\frac{d\varphi}{dx} = \sigma\frac{\lambda_o}{L} \tag{1}$$

where $d\varphi/dx$ indicates a suitable constant gradient along the metasurface and λ_o represents the wavelength in free space. Here, L represents the periodic length of the metasurface array for the 2π continuous phase gradient, and $\sigma = \pm 1$ corresponds to the helicity of left-handed circular polarization (LCP) and right-handed circular polarization (RCP) of incident light for one propagation direction.

Here, we only consider anomalous refraction for normal incident waves. Then, the anomalous refraction angle θ_t can be represented by

$$\theta_t = \arcsin\left(\sigma\frac{\lambda_o}{n_t L}\right) \tag{2}$$

This angular shift will induce a real-space shift s, which increases linearly with the wave transmission distance d (distance perpendicular to the metasurface), such that

$$s = d \times \tan\theta_t \tag{3}$$

According to Equation (2), the refraction angle θ_t assumes opposite values for LCP and RCP waves, which means the LCP and RCP conversion wave will be separated and propagate along two directions. This behavior is the PSHE based on the geometric phase gradient.

The efficiency of the PSHE based on the geometric phase gradient will be discussed next. If a light beam passes through a medium with coordinate-related geometric phase gradient, the spin-to-orbital angular momentum conversion will take place. According to Equation (1), this phase gradient is defined as a spin Hall momentum offset $k_x = \frac{d\varphi}{dx}$. The coordinate-related geometric phase gradient in a metasurface for LCP and RCP waves is always obtained by polarization conversion effect in gold nanorod-based unit cells. Thus, the efficiency of PSHE is directly associated with the polarization conversion efficiency of each unit cell. The optical function of a gold nanorod can always be treated as an imperfect polarizer, which can be represented by the Jones matrix $\mathbf{T}$,[29,30] such that

$$\mathbf{T}_{lin} = \begin{pmatrix} T_{xx} & T_{xy} \\ T_{yx} & T_{yy} \end{pmatrix} = \begin{pmatrix} A & 0 \\ 0 & 0 \end{pmatrix} \tag{4}$$

where $0 < A \leq 1$. Here, we assume that the optical axis of the nanorod lies along the x-direction. Then, the Jones matrix $\mathbf{T}$ of a nanorod that makes an angle θ with the x-direction can be expressed as

$$\mathbf{T}_{lin}^{\theta} = \mathbf{R}(-\theta)\mathbf{T}_{lin}\mathbf{R}(\theta) = A\begin{pmatrix} \cos^2\theta & \sin\theta\cos\theta \\ \sin\theta cos\theta & \sin^2\theta \end{pmatrix} \tag{5}$$

where

$$\mathbf{R}(\theta) = \begin{pmatrix} \cos\theta & \sin\theta \\ -\sin\theta & \cos\theta \end{pmatrix} \tag{6}$$

Then, for the circular polarization base, the Jones matrix $\mathbf{T}_{lin}^{\theta}$ can be rewritten as

$$\mathbf{T}_{circ}^{\theta} = \frac{A}{2}\begin{pmatrix} 1 & e^{-i2\theta} \\ e^{i2\theta} & 1 \end{pmatrix} \tag{7}$$

Next, we consider a linear-polarized (LP) incident wave for which the Jones vector $\mathbf{J}$ is

$$\mathbf{J}_{in} = \begin{pmatrix} E_{LCP} \\ E_{RCP} \end{pmatrix} = \frac{\sqrt{2}}{2}\begin{pmatrix} 1 \\ 1 \end{pmatrix} \tag{8}$$

Then, the Jones vector of the refraction wave is given by

$$\begin{aligned} \mathbf{J}_{refractions} &= \mathbf{T}_{circ}^{\theta}\mathbf{J}_{in} = \mathbf{J}_{refraction}^{anomalous} + \mathbf{J}_{refraction}^{normal} \\ &= \frac{\sqrt{2}A}{4}\begin{pmatrix} e^{-i2\theta} \\ e^{i2\theta} \end{pmatrix} + \frac{\sqrt{2}A}{4}\begin{pmatrix} 1 \\ 1 \end{pmatrix} \end{aligned} \tag{9}$$

Here, $\mathbf{J}_{refraction}^{anomalous}$ indicates the anomalous refraction occurring while a continuous geometric phase gradient is generated by using a series of nanorods with rotating angles from 0 to π. The transmission wave includes both anomalous refraction $\mathbf{J}_{refraction}^{anomalous}$ and normal refraction $\mathbf{J}_{refraction}^{normal}$. In this circumstance, the efficiency of the anomalous refraction is no greater than 25%, which has been experimentally confirmed.[31] Therefore, both the existence of normal refraction and the limits on efficiency prevent gold-nanorod-based metasurfaces from achieving high-performance PSHE.

However, these drawbacks can be overcome if the optical function of the gold nanorod can be designed as a half-wave plate. Different from metasurface designs based on dielectric materials, gold nanorod should be considered as an imperfect half-wave plate rather than a half-wave plate because of the existence of ohmic losses.[32,33] The Jones matrix of an imperfect half-wave plate can be expressed by

$$\mathbf{T}'_{\text{lin}} = \begin{pmatrix} T_{xx} & T_{xy} \\ T_{yx} & T_{yy} \end{pmatrix} = \begin{pmatrix} B & 0 \\ 0 & -C \end{pmatrix} \tag{10}$$

where $0 < B \leq 1$ and $0 < C \leq B$. The imperfect half-wave plate can be treated as a combination of a perfect half-wave plate and a perfect polarizer, where

$$\begin{aligned} \mathbf{T}'_{\text{lin}} &= \begin{pmatrix} T_{xx} & T_{xy} \\ T_{yx} & T_{yy} \end{pmatrix} = \begin{pmatrix} B & 0 \\ 0 & -C \end{pmatrix} \\ &= C\begin{pmatrix} 1 & 0 \\ 0 & -1 \end{pmatrix} + (B-C)\begin{pmatrix} 1 & 0 \\ 0 & 0 \end{pmatrix} \end{aligned} \tag{11}$$

Then, for a circular polarization base, the corresponding Jones matrix $\mathbf{T}'^{\theta}_{\text{lin}}$ of the nanorod making an angle θ with the x-direction can be written as

$$\mathbf{T}'^{\theta}_{\text{circ}} = C\begin{pmatrix} 0 & e^{-i2\theta} \\ e^{i2\theta} & 0 \end{pmatrix} + \frac{(B-C)}{2}\begin{pmatrix} 1 & e^{-i2\theta} \\ e^{i2\theta} & 1 \end{pmatrix} \tag{12}$$

Then, when we consider a LP incident wave as shown in Equation (8), the refraction wave is given by

$$\begin{aligned} \mathbf{J}'_{\text{refractions}} &= \mathbf{T}'^{\theta}_{\text{circ}}\,\mathbf{J}_{\text{in}} = \mathbf{J}'^{\text{anomalous}}_{\text{refraction}} + \mathbf{J}'^{\text{normal}}_{\text{refraction}} \\ &= \frac{\sqrt{2}}{4}(B+C)\begin{pmatrix} e^{-i2\theta} \\ e^{i2\theta} \end{pmatrix} + \frac{\sqrt{2}}{4}(B-C)\begin{pmatrix} 1 \\ 1 \end{pmatrix} \end{aligned} \tag{13}$$

If the condition $B = C = 1$ is satisfied, the performance of the gold nanorod can be treated as a perfect half-wave plate and no normal refraction exists. In this situation, the efficiency of PSHE can reach 100%. Thus, the high-performance PSHE based on geometric phase gradients can be achieved by designing a gold-nanorod-based metasurface whose optical function of each unit cell can be regarded as a near-perfect half-wave plate. Moreover, this desirable design can also produce complete polarization conversion without recourse to rotating nanorods.

The proposed gold-nanorod-based near-perfect half-wave plate can satisfy the abovementioned conditions and produce a high-performance PSHE. **Figure 1**a shows the performance of the proposed nanorod. The transmission spin (σ_+ or σ_-) opposes the incident beam because of the π phase delay along the x-axis, which is induced by the anisotropic optical resonance mode of the nanorod. SiO_2 was used as the substrate with 4000 nm in the simulation, and the gold nanorod was designed to be 290 nm thick with a 100 nm thick SiO_2 layer covering it. The periods of the unit cell are all $P = 500$ nm along the x- and y-directions, while the designed nanorod has dimensions of length $U = 335$ nm and width $W = 100$ nm. Figure 1b presents a graphical rendering that shows the generation of the PSHE with the proposed gold-nanorod-based metasurface. Numerical simulations have been conducted to analyze the characteristics of the proposed nanorod and nanorod-based metasurface. These simulations were carried out by using the finite differential time domain (FDTD) method. In our simulation, periodic boundary conditions were used in the x- and y-directions representing a periodical structure. The perfectly matched layers were used at the top and the bottom (bottom of substrate) of the simulation domain, leaving the simulation domain in the direction of propagation. The permittivity of the SiO_2 was set at 2.16, and the permittivity of gold was described by the Drude model after fitting the experimental data.[34]

First, we discuss the polarization conversion performance and anisotropic optical resonance mode of the designed nanorod. **Figure 2**a shows the simulation results for the transmission coefficient magnitudes $|T_{xx}|$ and $|T_{yy}|$ of the designed nanorod, while Figure 2b depicts the simulation results of the transmission coefficient phases φ_{xx} and φ_{yy} and the corresponding phase difference $\Delta\varphi = \varphi_{yy} - \varphi_{xx}$. As indicated by Equation (10), the performance of the designed gold nanorod can be treated as a near-perfect half-wave plate at a wavelength of 1067 nm. Then, its Jones matrix can be expressed as

$$\mathbf{T}'_{\text{lin}} = \begin{pmatrix} T_{xx} & T_{xy} \\ T_{yx} & T_{yy} \end{pmatrix} = \begin{pmatrix} 0.976 & 0 \\ 0 & -0.850 \end{pmatrix} \tag{14}$$

The polarization conversion performance of the proposed nanorod can be shown visually by expressing the simulation results of transmission coefficient magnitudes $|T_{ll}|$ and $|T_{rl}|$ and the polarization conversion rate (PCR) as

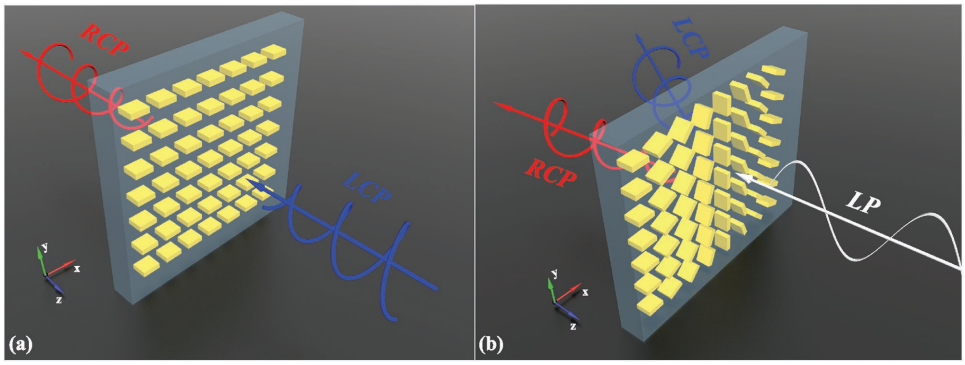

Figure 1. Schematic of the designed gold-nanorod-based metasurfaces. a) A rendering of the near-perfect circular-to-circular polarization conversion in a nanorod array. The proposed nanorod array induces a π phase delay along the x-axis, which causes the LCP or RCP spin of transmission to be opposed to the incident light. b) A depiction of the PSHE in a nanorod-based metasurface. A transmitted linear-polarized incident beam will be divided into two parts with two propagation directions and opposite spins.

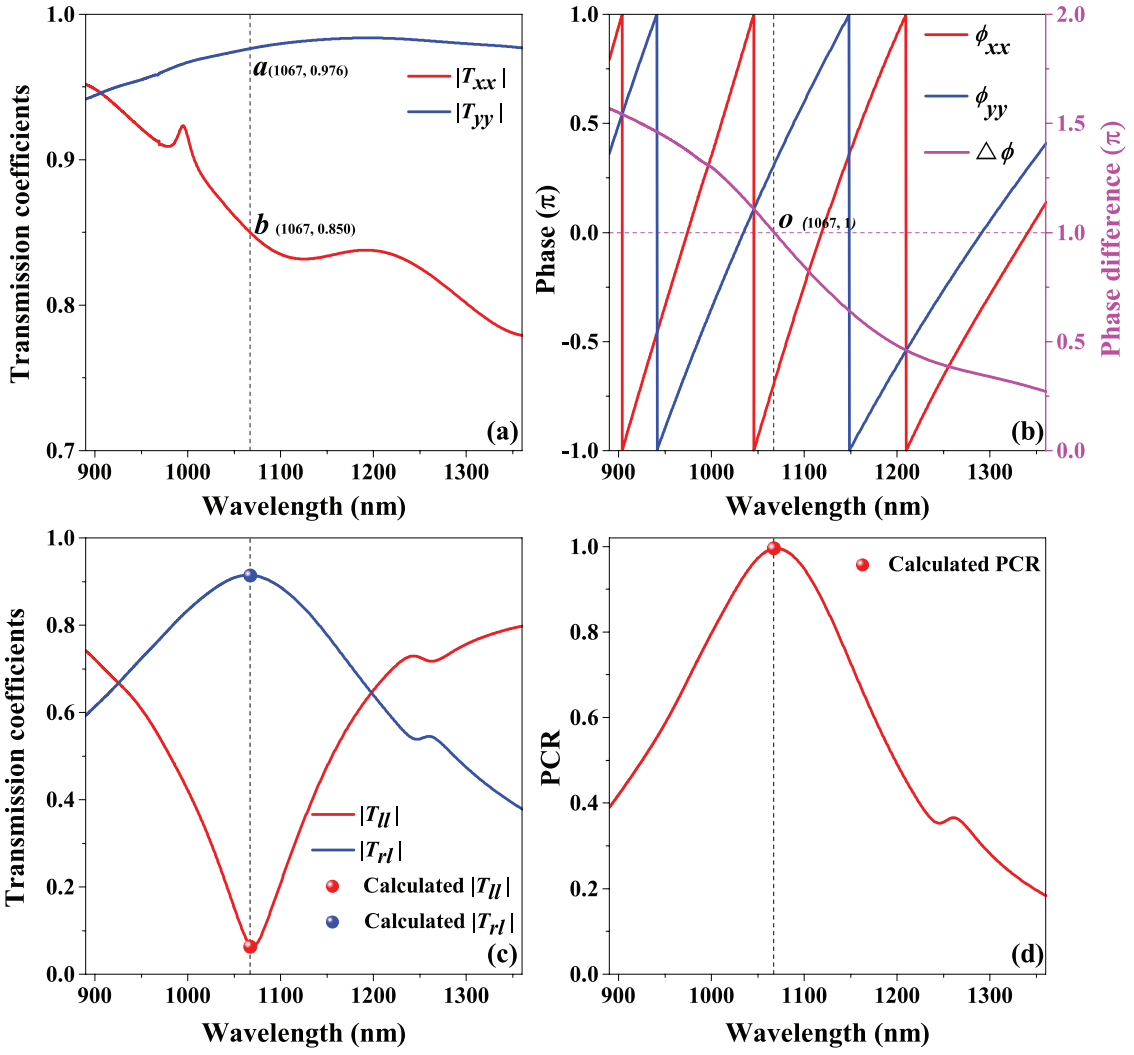

Figure 2. Polarization conversion performance of the proposed nanorod. a) The simulation results of the transmission coefficient magnitudes $|T_{xx}|$ and $|T_{yy}|$. b) The simulation results of the transmission coefficient phases φ_{xx} and φ_{yy} and the corresponding phase difference $\Delta\varphi = \varphi_{yy} - \varphi_{xx}$. c) The simulation results of the transmission coefficient magnitudes $|T_{ll}|$ and $|T_{rl}|$ and the transmission coefficient magnitudes calculated for a wavelength of 1067 nm. d) The simulation results of PCR and the values of PCR calculated for a wavelength of 1067 nm.

$$\mathrm{PCR} = \frac{|T_{rl}|^2}{|T_{ll}|^2 + |T_{rl}|^2} \tag{15}$$

Results are depicted in Figure 2c,d. The cross-polarized transmission coefficient $|T_{rl}|$ is over 0.9, and the copolarized transmission coefficient $|T_{ll}|$ is almost 0 at 1067 nm. The transmission intensity is equal to the square of the transmission coefficient. According to Figure 2c, the transmission intensity of cross-polarized wave is over 0.8 at 1067 nm, which indicates that the sum of the optical loss and the reflection intensity is no more than 0.2 in the designed wavelength. Also, the PCR at 1067 nm is almost 1, which means the polarization states of transmission and incidence are opposite at almost 100% polarization-conversion efficiency. The calculated transmission coefficient magnitudes $|T_{ll}|$ and $|T_{rl}|$ and the corresponding PCR depend on Equations (12) and (15) at 1067 nm. These results also appear in Figure 2c,d and agree well with the simulated results. The realization of this near-perfect half-wave plate can be attributed to the anisotropic optical resonance mode in the designed nanorod. According to Figure 2a, the interaction between the incident beam and the nanorod induced an optical resonance along the *x*-axis while yielding almost no optical resonance along the *y*-axis, which result in a π phase delay in the *x*-direction.

The simulated time snapshots of current densities and distributions of the electric field component E_x at 1067 and 1360 nm are shown in **Figure 3**a,b, respectively, show the underlying physics of this phase delay produced in the *x*-direction by the optical resonance of the designed nanorod. Different from previous ultrathin metasurfaces whose thickness are nearly an order of magnitude smaller than the working wavelength, the thickness of the proposed structures can be compared with the working wavelength, which results in a new oscillation mode of electrons. The oscillation of electrons at 1067 nm no longer occurs along the *x*-axis of the nanorod. Rather, the oscillation

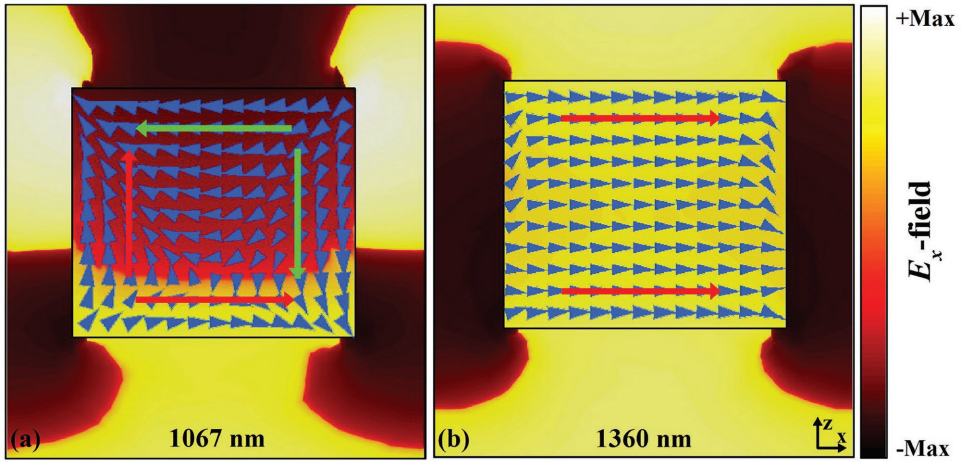

Figure 3. Schematic of the polarization conversion in a nanorod. The simulated time snapshots of current densities and distributions of the electric field component E_x at a) 1067 and b) 1360 nm.

has a component along the wave-propagation direction when compared with its properties at 1360 nm. The oscillation component along the wave-propagation direction induces a π phase change of the electric field component E_x in the near field, which lead to the optical function of the proposed structures can be regarded as a near-perfect half-wave plate rather than

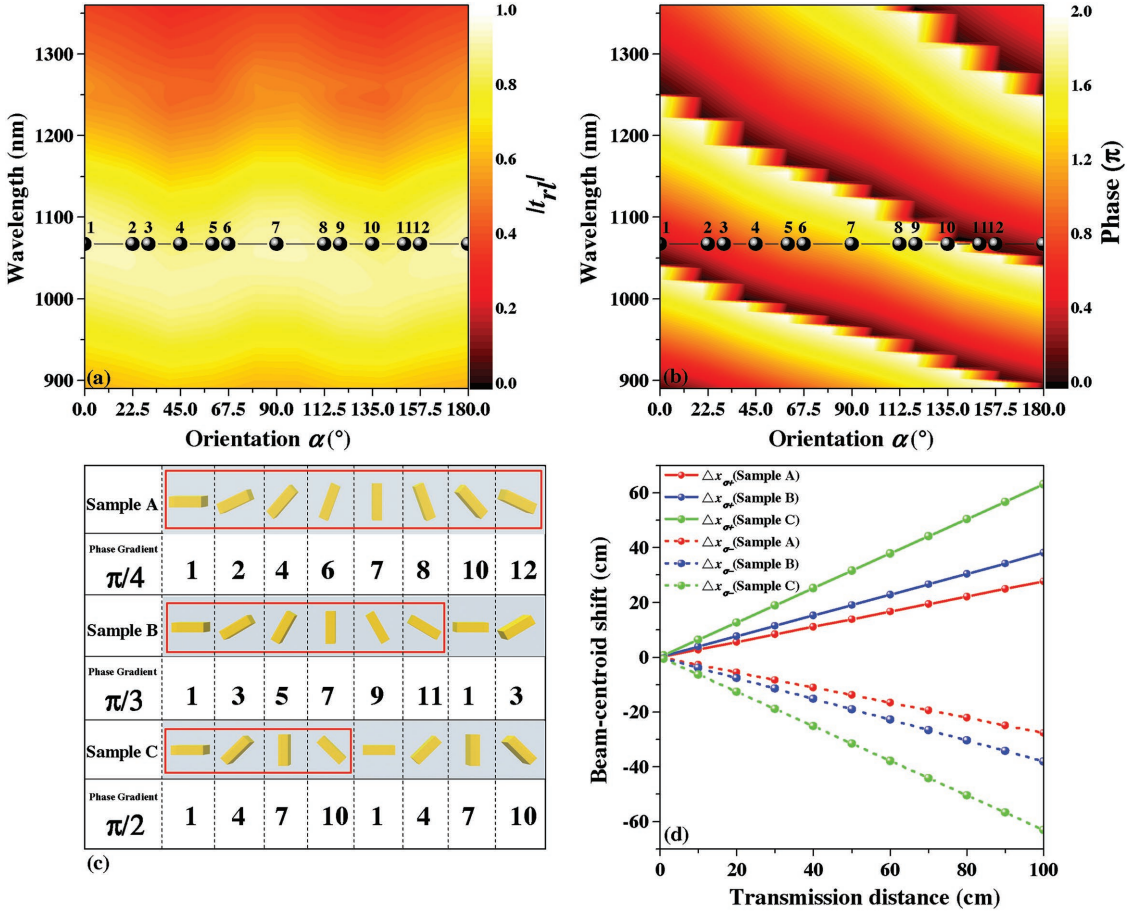

Figure 4. Phase and PSHE manipulation in a gold-nanorod-based metasurfaces. The simulation results of cross-polarized transmission coefficient a) magnitude $|T_{rl}|$ and b) phase of the nanorod for different orientation angles α, the angle between the long axis of the nanorod and the *x*-axis. c) The designed nanorod-based metasurface with different phase gradients. d) The calculated beam-centroid shift of the PSHE for different transmission distances in a nanorod-based metasurface with different phase gradients.

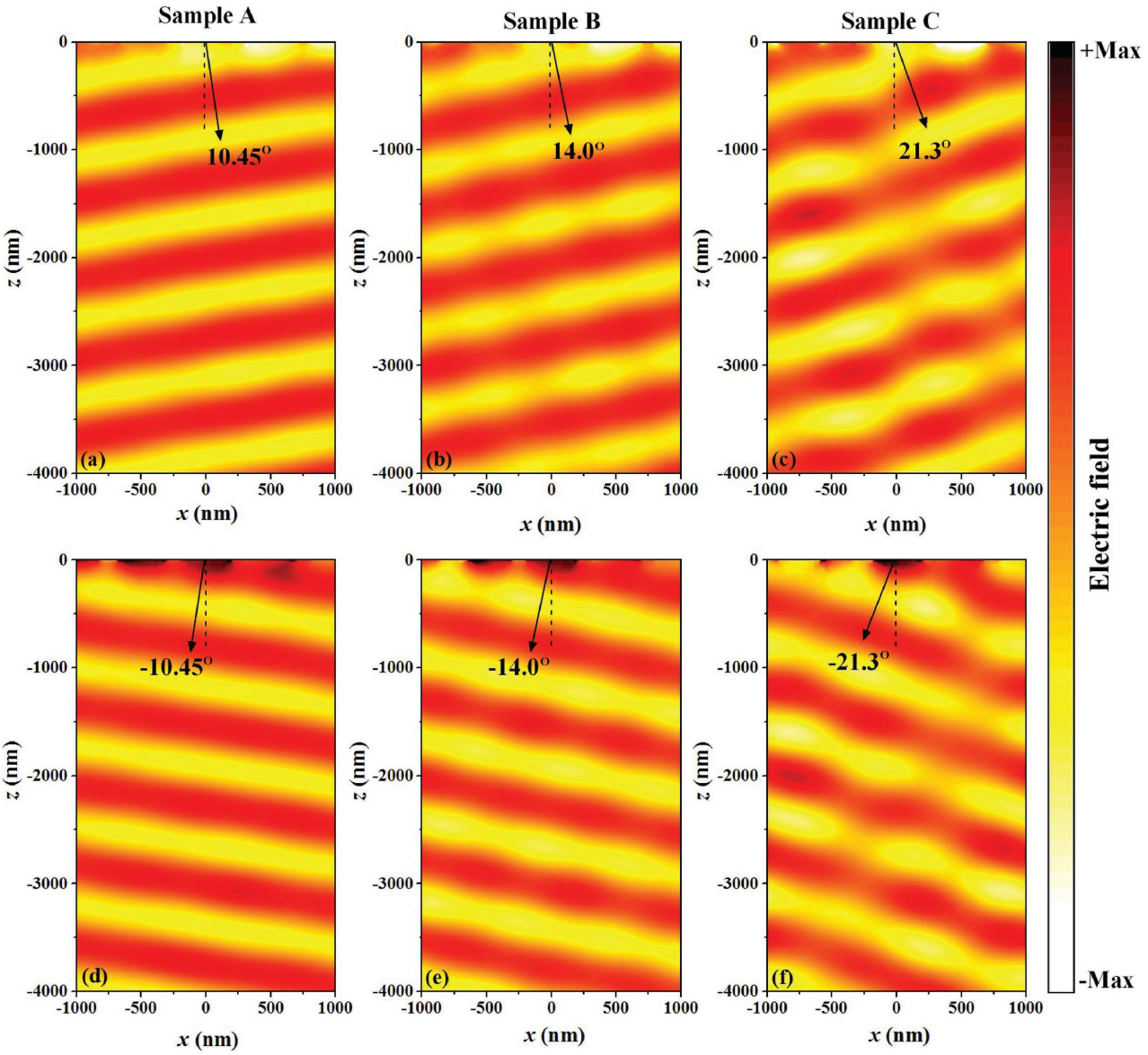

Figure 5. Manipulation of the PSHE in a nanorod-based metasurface with different phase gradients. a–c) The simulated time snapshots of electric field maps of transmission for LCP with Samples A through C of nanorod-based metasurfaces with different phase gradients, respectively. d–f) The simulated time snapshots of electric field maps of transmission for RCP with Samples A through C of nanorod-based metasurfaces with different phase gradients, respectively.

an imperfect polarizer and can result in a high-performance PSHE.

According to Equations (1) and (7), the instances of the PSHE in metasurfaces attributed to the phase gradient along the metasurfaces always are generated by changing structure orientations. The simulation results for the cross-polarized transmission coefficient magnitude $|T_{rl}|$ and phase of the designed nanorod for different orientation angles α, the angle between the long axis of the nanorod and the x-axis, appear in **Figure 4**a,b. Even though the initial phase differs for varying wavelengths, the generated phase gradient and orientation angle follow the linear relation $\Delta\theta = 2\alpha$ for any wavelength. Thus, the 2π phase gradient can be produced by changing the orientation angle α in the range from 0 to π as shown in Figure 4b. Moreover, the cross-polarized transmission coefficient $|T_{rl}|$ varies slightly with changes in the orientation angle; this property implies that the wave vector of a cross-polarized transmission can be manipulated by metasurfaces with a 2π phase gradient while maintaining high efficiency. According to Equations (1) through (3), the anomalous refraction angle θ_t and the real-space shift s of the cross-polarized transmission are attributable to the periodic length L of the metasurface array for the 2π phase gradient, which means the PSHE can be manipulated by varying L. Figure 4c shows designs of three nanorod-based metasurfaces with 2π phase gradients along the x-axis (as shown in Figure 1b) and different periodic

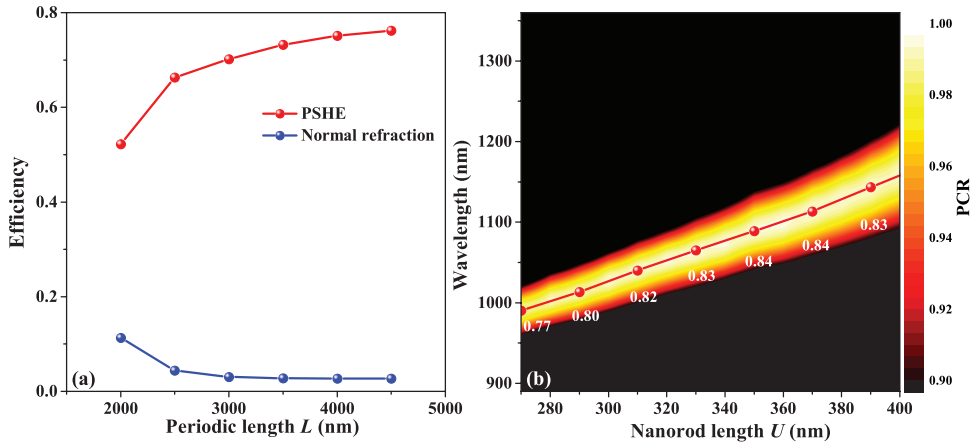

Figure 6. a) Simulated efficiency of PSHE and normal refraction for nanorod-based metasurfaces with different periodic length L at 1067 nm. b) Simulated PCR for different nanorod lengths U. The maximum value of PCR with corresponding transmission intensity $t_{rl} = |T_{rl}|^2$ of cross-polarized wave (shown as white numbers) for different nanorod lengths are given by red dotted line. The working wavelength of the proposed nanorod-based near-perfect half-wave plate can be manipulated by intentionally varying the nanorod lengths.

lengths L. Here, Sample A uses $L = 4000$ nm with $\Delta\varphi = \pi/4$, Sample B uses $L = 3000$ nm with $\Delta\varphi = \pi/3$, and Sample C uses $L = 2000$ nm with $\Delta\varphi = \pi/2$. Figure 4d then shows the calculated results of the beam-centroid shift of the PSHE for different transmission distances in air at 1067 nm for the three metasurface designs. Here, different periodic lengths L can manipulate the wave vector of cross-polarized transmissions, and different transmission distances can vary the beam-centroid shift. Furthermore, the PSHE can be reversed by reversing the incident beam direction because the phase gradient reverses its direction when the incident direction is reversed. The use of the proposed nanorod-based near-perfect half-wave plate permits easy and arbitrary manipulation of the PSHE with high efficiency around 1067 nm.

Figure 5 presents time snapshots of electric-field map of transmission with LCP and RCP for the designed metasurfaces at 1067 nm. This representation visualizes the manipulation of the PSHE in the designed metasurfaces. The wave vector is effectively manipulated by adjusting the periodic length L; the obtained results are consistent with the theoretical predictions. Although the conversion efficiency of each unit cell is near 100%, it does not mean the beam refracting surface is exactly as the designed behavior due to undesired evanescent coupling between the different cells. Thus, we simulated the efficiency (relative to the incident intensities) of PSHE and normal refraction with infinite array and different periodic length L in **Figure 6**a. The high-order diffractions for anomalous refraction are not given as their intensities are close to zero when L is larger than 2000 nm and no more than 3% when L is equal to 2000 nm (Sample C). As the enhancement of the undesired evanescent coupling induced by the increasing of phase gradient, the efficiency of PSHE and the normal refraction will, respectively, decrease and increase with the decreasing of the periodic length. The efficiency of normal refraction is almost 0 when L is larger than 2000 nm and no more than 12% in Sample C, which indicates that the incident light with an arbitrary polarization state can undergo nearly complete conversion into two refraction waves with opposite spin states and opposite spin-dependent wave-vector shifts. Furthermore, the efficiency of PSHE in Sample A is over 70% and the efficiency of PSHE in all three designs is over 50%. Such high efficiency of PSHE in refraction has not yet been reported in single-layer gold-structure-based metasurfaces.

According to Figure 2b, the designed nanorod can be treated as a near-perfect half-wave plate only around 1067 nm with a phase delay of $\Delta\varphi = \pi$. At other wavelengths, the PSHE still exists for cross-polarized transmissions coefficient not equal to 0, but the conversion efficiency no longer approaches 100%. However, the working wavelength of a nanorod-based near-perfect half-wave plate can be easily adjusted by changing the structural parameters of the nanorod. Figure 6b shows the wavelength selection process by depicting the simulated results of PCR for different nanorod lengths U. The waveband of PCR > 90% can be easily manipulated by varying the nanorod length U while keeping high transmission intensity of cross-polarized wave, as shown by the red dotted line. This result also indicates that the imperfectness in further fabrication process will only cause a slight changing of the position of the conversion peak while keeping its value, which is also beneficial to the real application of the proposed metasurface. When the working wavelength is not near 1067 nm, to keep the performance of the designed nanorod, several structural parameters must be adjusted.

The PSHE falls into one of the basic classes of phenomena involving photonic spin–orbit interactions. These interactions have attracted growing interest in modern nanophotonics because of their crucial role in determining the behavior of light at subwavelength scales. However, conventional approaches to generating the PSHE always require bulky systems and exhibit very low efficiencies, thereby complicating their use in practical applications. Fortunately, metasurfaces provide an effective method for overcoming the drawbacks of conventional approaches to manipulating photon spin and orbital angular momentum.

In summary, we presented the basic theory, a simulated demonstration, and a comprehensive analysis of a giant PSHE in refraction with over 70% efficiency in a gold-nanorod-based metasurface. Theoretical analyses indicate that nanorods

treated as near-perfect half-wave plates can be used to produce large-scale instances of the PSHE. The results of the theoretical analysis can be used to guide designs of gold-nanorod-based and several nanorod-based metasurfaces, and optimize the giant PSHE in refraction. The simulation results, consistent with the theoretical prediction, showed that a giant PSHE could be realized at a wavelength of 1067 nm with efficiency over 70%. Incident light with an arbitrary polarization state can undergo nearly complete conversion into two refraction waves with opposite spin states and opposite spin-dependent wave-vector shifts. The high efficiency and integration of the designs overcame the inherent defects of known conversion approaches, thereby enabling such metasurfaces to be used in practical applications. Moreover, the spin-dependent wave-vector shifts and beam-centroid shifts of the converted refraction waves could be effectively manipulated by changing the periodic lengths of the proposed metasurfaces and the transmission distances. An application of this method for adjusting parameters further improved the performance of the proposed metasurfaces and broadened their range of potential applications. These proposed and demonstrated concepts may prove applicable in various uses of spin-controlled nanophotonics, such as optical communications, beam splitting, spin selection, and spin-dependent holographic imaging.

Acknowledgements

This work was supported by the National Key Research and Development Program of China (2016YFA0301102), the Natural Science Foundation of China (11574163 and 61378006), and the Program for New Century Excellent Talents in University (NCET-13-0294). The authors also acknowledge the support from the Collaborative Innovation Center of Extreme Optics, Shan Xi University, Taiyuan, Shanxi, China.

Conflict of Interest

The authors declare no conflict of interest.

Keywords

half-wave plate, high efficiency, manipulation, photonic spin Hall effect

Received: May 2, 2017
Revised: June 19, 2017
Published online:

[1] F. Cardano, L. Marrucci, *Nat. Photonics* **2015**, *9*, 776.
[2] K. Y. Bliokh, F. J. Rodríguez-Fortuño, F. Nori, A. V. Zayats, *Nat. Photonics* **2015**, *9*, 796.
[3] L. B. Ma, S. L. Li, V. M. Fomin, M. Hentschel, J. B. Götte, Y. Yin, M. R. Jorgensen, O. G. Schmidt, *Nat. Commun.* **2016**, *7*, 10983.
[4] X. Ling, X. Zhou, K. Huang, Y. Liu, C. W. Qiu, H. Luo, S. Wen, *Rep. Prog. Phys.* **2017**, *80*, 066401.
[5] Y. Liu, Y. Ke, H. Luo, S. Wen, *Nanophotonics* **2017**, *6*, 51.
[6] K. Y. Bliokh, Y. P. Bliokh, *Phys. Rev. Lett.* **2006**, *96*, 073903.
[7] O. Hosten, P. Kwiat, *Science* **2008**, *319*, 787.
[8] Y. Qin, Y. Li, H. Y. He, Q. H. Gong, *Opt. Lett.* **2009**, *34*, 2551.
[9] M. Onoda, S. Murakami, N. Nagaosa, *Phys. Rev. Lett.* **2004**, *93*, 083901.
[10] L. Zhang, S. Mei, K. Huang, C. W. Qiu, *Adv. Opt. Mater.* **2016**, *4*, 818.
[11] H. Cheng, Z. Liu, S. Chen, J. Tian, *Adv. Mater.* **2015**, *27*, 5410.
[12] Y. Fan, N. H. Shen, T. Koschny, C. M. Soukoulis, *ACS Photonics* **2015**, *2*, 151.
[13] B. Xu, C. Wu, Z. Wei, Y. Fan, H. Li, *Opt. Mater. Express* **2016**, *6*, 3940.
[14] Y. Fan, N. H. Shen, F. Zhang, Z. Wei, H. Li, Q. Zhao, Q. Fu, P. Zhang, T. Koschny, C. M. Soukoulis, *Adv. Opt. Mater.* **2016**, *4*, 1824.
[15] X. Ling, X. Zhou, X. Yi, W. Shu, Y. Liu, S. Chen, H. Luo, S. Wen, D. Fan, *Light: Sci. Appl.* **2015**, *4*, e290.
[16] X. Ling, X. Zhou, W. Shu, H. Luo, S. Wen, *Sci. Rep.* **2014**, *4*, 5557.
[17] X. Yin, Z. Ye, J. Rho, Y. Wang, X. Zhang, *Science* **2013**, *339*, 1405.
[18] Y. Liu, X. Ling, X. Yi, X. Zhou, S. Chen, Y. Ke, H. Luo, S. Wen, *Opt. Lett.* **2015**, *40*, 756.
[19] Y. Li, Y. Liu, X. Ling, X. Yi, X. Zhou, Y. Ke, H. Luo, S. Wen, D. Fan, *Opt. Express* **2015**, *23*, 1767.
[20] S. Wang, X. Wang, Q. Kan, J. Ye, S. Feng, W. Sun, P. Han, S. Qu, Y. Zhang, *Opt. Express* **2015**, *23*, 26434.
[21] B. Desiatov, N. Mazurski, Y. Fainman, U. Levy, *Opt. Express* **2015**, *23*, 22611.
[22] W. Shu, Y. Ke, Y. Liu, X. Ling, H. Luo, X. Yin, *Phys. Rev. A* **2016**, *93*, 013839.
[23] J. Jin, J. Luo, X. Zhang, H. Gao, X. Li, M. Pu, P. Gao, Z. Zhao, X. Luo, *Sci. Rep.* **2016**, *6*, 24286.
[24] W. Luo, S. Xiao, Q. He, S. Sun, L. Zhou, *Adv. Opt. Mater.* **2015**, *3*, 1102.
[25] J. Li, S. Chen, H. Yang, J. Li, P. Yu, H. Cheng, C. Gu, H.-T. Chen, J. Tian, *Adv. Funct. Mater.* **2015**, *25*, 704.
[26] Z. Liu, Z. Li, Z. Liu, J. Li, H. Cheng, P. Yu, W. Liu, C. Tang, C. Gu, J. Li, S. Chen, J. Tian, *Adv. Funct. Mater.* **2015**, *25*, 5428.
[27] N. Yu, P. Genevet, M. A. Kats, F. Aieta, J.-P. Tetienne, F. Capasso, Z. Gaburro, *Science* **2011**, *334*, 333.
[28] H. Cheng, S. Chen, P. Yu, W. Liu, Z. Li, J. Li, B. Xie, J. Tian, *Adv. Opt. Mater.* **2015**, *3*, 1744.
[29] L. Huang, X. Chen, H. Mühlenbernd, G. Li, B. Bai, Q. Tan, G. Jin, T. Zentgraf, S. Zhang, *Nano Lett.* **2012**, *12*, 5750.
[30] X. Chen, L. Huang, H. Mühlenbernd, G. Li, B. Bai, Q. Tan, G. Jin, C.-W. Qiu, S. Zhang, T. Zentgraf, *Nat. Commun.* **2012**, *3*, 1198.
[31] X. Ding, F. Monticone, K. Zhang, L. Zhang, D. Gao, S. N. Burokur, A. Lustrac, Q. Wu, C.-W. Qiu, A. Alù, *Adv. Mater.* **2015**, *27*, 1195.
[32] M. Khorasaninejad, K. B. Crozier, *Nat. Commun.* **2014**, *5*, 5386.
[33] M. Khorasaninejad, W. T. Chen, R. C. Devlin, J. Oh, A. Y. Zhu, F. Capasso, *Science* **2016**, *352*, 1190.
[34] E. D. Palik, *Handbook of Optical Constant of Solids*, Academic Press, San Diego, CA **1985**.